Colloid Polym Sci (2016) 294:833–840
DOI 10.1007/s00396-016-3836-4

ORIGINAL CONTRIBUTION

Investigation of Cassie-Wenzel Wetting transitions on microstructured surfaces

Tai-min Cai[1] · **Zhi-hai Jia**[1] · **Hui-nan Yang**[1] · **Gang Wang**[1]

Received: 21 August 2015 / Revised: 15 January 2016 / Accepted: 25 January 2016 / Published online: 12 February 2016

Abstract Understanding the physical mechanism of wetting transitions is crucial for the design of highly stable superhydrophobic materials. Wetting transitions from Cassie state to Wenzel state on microstructured surfaces were investigated in this article. The pinning force τ was introduced to establish a new mechanical equilibrium, obtaining the model of critical pressure p_c of Cassie-Wenzel wetting transition and the model was qualitatively verified by performing a series of experiments. Using the model of p_c and experimental data, the pinning force τ on different microstructured surfaces was obtained.

Keywords Wetting transitions · Pinning force · Microstructures surfaces

Introduction

Superhydrophobic materials are prevailing in numerous fields because of their special characteristics, such as anti-adhesion [1, 2], self-cleaning [3, 4], and anti-frost [4, 5]. In recent years, through photoetching [6, 7], spraying and coating [8], and chemical corrosion [9], superhydrophobic surfaces emerge abundantly [10, 11]. However, the instability of hydrophobicity still restricts widespread application of superhydrophobic material [7, 12–15]. A droplet suspends on the top of microstructures, forming the nonwetted Cassie-Baxter state, but it tends to permeate into microgrooves, forming the fully wetted Wenzel state. In order to guarantee the stability of hydrophobicity, researchers induce droplets to accomplish Wenzel-Cassie wetting transition through additional vibration [16, 17], heating [18, 19], electricity [20, 21], and magnetism [22]. Nevertheless, maintaining hydrophobicity by these approaches by external forces is only applicable to special occasions and leads to additional energy consumption. Therefore, it is necessary to study the mechanism of Cassie-Wenzel wetting transition and explore an optimum geometric size and shape of microstructures to obtain a more stable superhydrophobic surface.

At present, the Cassie-Wenzel wetting transition was extensively studied theoretically and experimentally [23–31]. Zheng et al. [23] determined the critical pressure p_c of Cassie-Wenzel wetting transition through force analysis on Cassie-Baxter droplet:

$$p_c = -\frac{4\gamma_{LV} f \cos\theta_Y}{(1-f)a} \tag{1}$$

where f is the fraction of solid on apparent wetted area, a is the side length of microstructure, γ_{LV} is the vapor-liquid interfacial tension, and θ_Y is the Young's or smooth-surface contact angle. When $\theta_Y \le 90°$ and $p_c \le 0$ Pa, the droplet cannot maintain the Cassie-Baxter state, which is discrepant from the experimental results in relevant literatures [32–34].

From various surface wetting phenomena, researchers [35–40] have noticed the pinning and depinning of three-phase contact lines, proposing the concept of pinning force. Some researchers studied the pinning phenomenon of Wenzel droplets [35, 36], Cassie droplets [37], and captive bubbles [38] in the case of advancing and receding. Pilat et al. [37] measured the forces required to slide sessile drops over surfaces by means of a vertical deflectable capillary stuck in the

✉ Zhi-hai Jia
zhhjia@usst.edu.cn

[1] School of Energy and Power Engineering, University of Shanghai for Science and Technology, Shanghai 200093, China

drop. Wu et al. [39] investigated the pinning and depinning mechanisms of the contact line during evaporation of nano-droplet sessile on textured surfaces using molecular dynamics method. However, the study on pinning phenomenon of droplets in wetting transition is relatively less. Bormashenko et al. [12, 30] realized the existence of an additional force on the brim of microstructure and established the value of the potential barrier for the displacement of the triple line as 10^{-6} J/m (1 μN) per unit length of the triple line from the perspective of the microstructure's shape angle. In our work, the pinning force will be considered as a variable, which is not only correlated to the microstructure's shape but also its size, and directly introduced into the model of Cassie-Wenzel wetting transition.

Experimental section

Samples Microstructured hydrophobic surfaces were prepared by photolithography on the substrate of polydimethylsiloxane (PDMS), and the Young's contact angle of water droplet was measured to be 109 ± 1° on the smooth PDMS surface. Scanning electron microscope (SEM) images of several typical samples were shown in Fig. 1. The microstructures were uniformly distributed in a rectangular grid, with three different heights h = 30, 55, and 60 μm shown in Fig. 1a–c and three different side lengths a = 20, 30, and 40 μm shown in Fig. 1d, a, e. There, in Fig. 1a–e, are about eight or nine different gaps b for each typical type, and the basic geometric parameters a, h, and b of microstructures are illustrated in Fig. 1f. In the sample preparation, a silicon wafer was first covered with SU8-25 photoresist layer of a fixed thickness by spin coating. Photolithography was then used to transfer the required pattern from a mask to the SU8-25 photoresist layer. The PDMS was then added to the mold, and they were together placed in the vacuum oven at 90 °C for 60 min. Finally, the PDMS polymer was separated from the SU8-25 photoresist layer to obtain the microstructured PDMS surfaces. It must be emphasized that we got unexpectedly the similar inverted trapezoid and similar trapezoid microstructured surfaces, as shown in Fig. 1a, c, d, while others were square pillar-like microstructured surfaces.

Measurement Experimental apparatus mainly include KINO SL200B-type contact angle measuring instrument (China), optical microscope, surface tensiometer, electronic scales, IDS 3370CP-C high-speed camera, and Netherlands FEI QUANTA FEG 450 field emission environmental scanning electron microscope (minimum resolution of 1 nm under low vacuum). The measured droplets were made of pure water and water-ethanol mixture of 4 μL. The temperature and relative humidity of the experimental environment was about 23.8 ± 2 °C and 46 ± 3 %, respectively.

Results and discussion

Pinning force As shown in Fig. 2, a water-ethanol mixture droplet of 4 μL was placed on the smooth surface and its equilibrium contact angle was 71 ± 1°, while the droplet was deposited gently on microstructured surfaces. The droplet in the Cassie state rested on top of the microstructures, with air

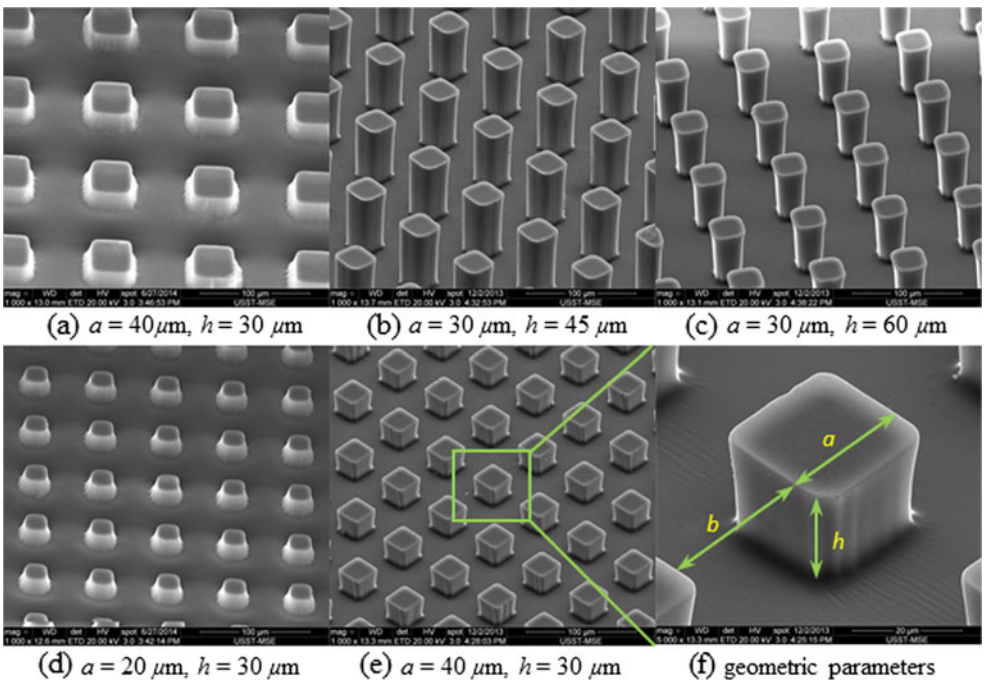

Fig. 1 Typical scanning electron microscope (SEM) images and geometric parameters of microstructured surfaces with different sizes of microstructures. Among them, **c** is one of the similar inverted trapezoid microstructured surfaces, while **a**, **d** and **b**, **e** are the representatives of similar trapezoid and square pillar-like microstructured surfaces, respectively. **f** illustrates the basic geometric parameters

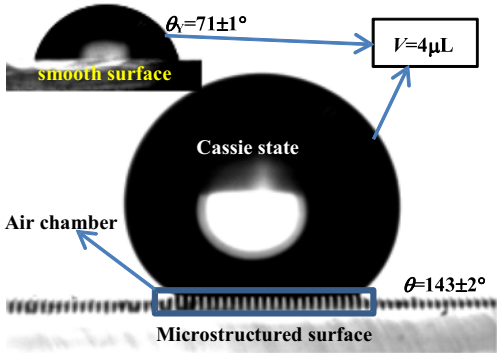

Fig. 2 Wetting state and contact angle of water-ethanol mixture droplets of 4 μL on the microstructured surface with a = 30 μm, b = 30 μm, and h = 60 μm, and its shape was shown in Fig. 2c. The *inset* depicts a droplet on the smooth surface

trapped underneath, as shown in Fig. 2, and its apparent contact angle reached 143 ± 2°. At this point, the traditional force analysis, such as Eq. 1, is not reasonable to explain the phenomenon. It was found that besides three interfacial tensions, there was an additional force on the top and side edge of a microstructure hindering the three-phase contact line from moving. It was called pinning force, denoted by τ, μN. Pinning force was related to not only the microstructure's geometric size but also its geometric shape.

As we know, the Young-Laplace's equation can be expressed as

$$\Delta P = \gamma_{LV}\left(\frac{1}{r_1}+\frac{1}{r_2}\right) \tag{2}$$

where ΔP is the pressure difference across the fluid interface, and r_1, r_2 are the principal radii of curvature. For a spherical cap, Eq. 2 can be simplified as

$$p_L = \frac{2\gamma_{LV}}{r} \tag{3}$$

where r is the radius of the spherical cap of a droplet and p_L is equivalent to ΔP, called Laplace's pressure for convenience here. The relative humidity η_g in microgrooves can be formulated as follows:

$$\eta_g \propto \frac{A_{cross}}{V_{space}} \tag{4}$$

where A_{cross} and V_{space}, respectively, denote the vapor-liquid interfacial area and air-vapor volume of a "cell" illustrated in Fig. 3f.

Geometric shape According to investigation results of Ahuja [40], almost all droplets (including pure alcohol) could stay suspended on the top of T-shape nanostructures and their apparent contact angles approached around 150°. The minimum radius r_{min} of curvature of the vapor-liquid interface near above the microgrooves reflects the amplitude of the critical pressure of the Cassie-Wenzel transition, because the smaller the minimum radius r_{min} is, the larger the Young-Laplace's pressure upward is according to Eq. 3. Comparing Fig. 3a–c, it was found that their A_{cross} were the same, but their V_{space} were different, leading to different relative humidity η_g. For the T-shape structure in Fig. 3a, the relative humidity η_g was smallest, so pinning force was at largest, while for the similar inverted-trapezoid in Fig. 3b and the pillar in Fig. 3c, pinning forces were at the second largest and the smallest, respectively.

In addition, the shape angle θ_s was formed by the microstructure's wall and original vapor-liquid interface denoted by the dashed line in Fig. 3. And it is significant to change the magnitude of pinning force. For example, as shown in Fig. 3a, the shape angle (θ_s) is 90° on the microstructures' top edge (point A). When the pressure surpasses the local critical pressure, the three-phase contact lines move to point B, where the shape angle is 180°. The "fakir" state kept until the pressure reached the larger critical pressure on point B. Under the same pressure, the larger the shape angle θ_s is, the farther the distance between the side wall and the curvature is, contributing to more difficulties for the curvature to contact the side wall. For the inverted-trapezoid in Fig. 3b, its shape angle is of $90° < \theta_s < 180°$. We fabricated the similar microstructured surfaces, which obtained better hydrophobicity than pillar-like and similar trapezoid microstructured surfaces, yet worse than the T-shape structured surface, under the same area fraction f. That is to say, the geometrical shape of the microstructure could change the magnitude of pinning force via regulating the shape angle θ_s.

Geometric size By comparison of Fig. 3c–e, it revealed that smaller side length a and larger height h caused greater pinning force. Under the same pressure, the radius of curvature of the vapor-liquid interface near above the microgrooves was identical according to Eq. 3, but difference exists on the pinning angle θ_{pin}, which was formed by the microstructure's wall and the tangent of the vapor-liquid interface denoted by the blue solid line in Fig. 3. Smaller pinning angle θ_{pin}, according to Eq. 4, possesses smaller relative humidity η_g. Therefore, a smaller scale of microstructure owns greater pinning force under the same f and h. Moreover, though A_{cross} could not be changed only by decreasing the height h of microstructure, V_{space} could be narrowed accordingly. Conformed with Eq. 4, the relative humidity η_g within the microgrooves in Fig. 3e increased consequently, contributing to less difficulty of movement of the three-phase contact lines. Thus, a larger height of microstructure resulted in a larger pinning force under the same f and a.

Wetting transition The force analysis of Cassie-Wenzel transition was shown in Fig. 4. For a droplet on microstructured

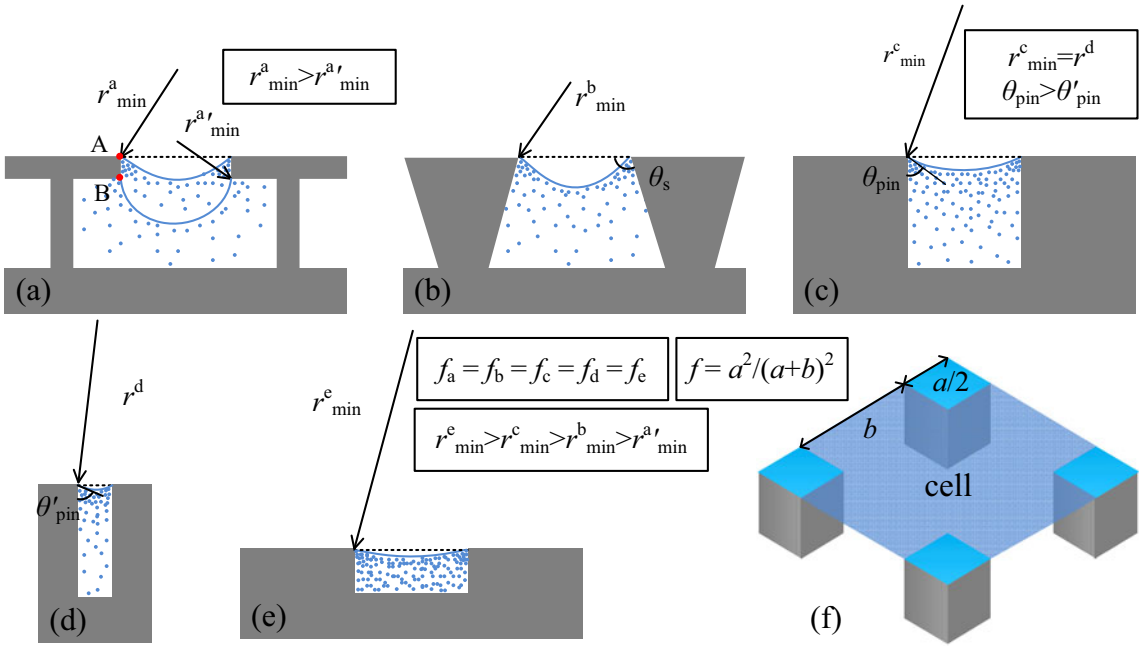

Fig 3 Schematic diagrams for effects of shape and size of microstructures on pinning force. Surfaces with **a** T-shape structures, **b** inverted-trapezoids, and **c**, **d**, **e** square pillars are with the same area fraction *f*. **c**, **d** are with the different pillar's side *a* and **c**, **e** with the different pillar's heights *h*. **f** denotes a "cell" for periodical structures

surfaces, the total downward force on the vapor-liquid interface was $(1-f)\pi r^2 p_c$ and the upward resultant force of single microstructure was $4a(\gamma_{SL}-\gamma_{SV})+\tau$, which was multiplied by the number of the microstructures in the wetted area $\pi r^2 f/a^2$, leading to the total upward force on the vapor-liquid interface equal to $(\tau-4a\gamma_{LV}\cos\theta_Y)\pi r^2 f/a^2$, where the Young's equation $\gamma_{SV}-\gamma_{SL}=\gamma_{LV}\cos\theta_Y$ and the definition $f=a^2/(a+b)^2$ have been applied.

The condition for transition onset, therefore, can be expressed in terms of the total force balance, which leads to, with the force moment ignored, the critical pressure p_c for Cassie-Wenzel transition:

$$p_c=\frac{f}{a(1-f)}\left(\frac{\tau}{a}-4\gamma_{LV}\cos\theta_Y\right) \quad (5)$$

which reflects the effect of microstructure on the robustness of hydrophobicity through not only the area fraction *f* and side length *a* but also the pinning force τ.

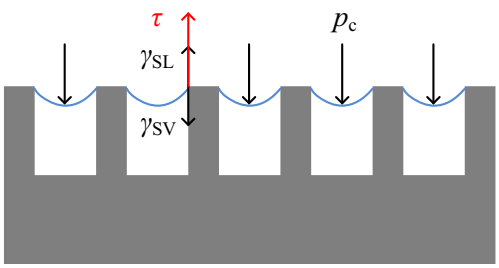

Fig. 4 Schematic diagram of force analysis for Cassie-Wenzel transition mode

The physical parameters (e.g., surface tension γ_{LV}, smooth-surface contact angle θ_Y, and density ρ) of the droplet can be utilized to verify Eq. 5 without any external force on a droplet. By regulating the proportion of ethanol in water-ethanol mixture by mass, we could obtain the droplet able to collapse into microgrooves to accomplish Cassie-Wenzel transition. Then, the water-ethanol mixture droplets were gently deposited on the different surfaces. When the transition on a microstructured PDMS surface just occurred, we recorded the surface tension, contact angle, and density of the droplet on the smooth PDMS substrate and, respectively, named them critical surface tension γ^c_{LV}, critical smooth-surface contact angle θ^c_Y, and critical density ρ^c. Therefore, the data were plotted in Fig. 5, in which the contact angle θ^c_Y denoted the difficulty of reaching wetting transition for pure water, i.e., the smaller the contact angle θ^c_Y was, the more hard the transition occurred.

Now, it is obviously revealed in Fig. 5 that with the area fraction *f* increasing, the transition occurred more difficultly. Furthermore, with decreasing of the height *h* in Fig. 5a, the transition occurred more easily under the same *f* and *a*. However, in Fig. 5b, the effects of the different side lengths *a* on the transition was somewhat interesting. The contact angles θ^c_Y of different surfaces with $a=20$, 40 μm (similar trapezoid) were almost all bigger than 90°, while those of the ones with $a=30$ μm (square pillar-like) were all smaller than 90°, which was notably caused by the microstructure's shape. Moreover, by the comparison of the microstructured surfaces with $a=20$ and 40 μm (similar trapezoid), it was confirmed that the smaller the side length *a* was, the more difficultly the

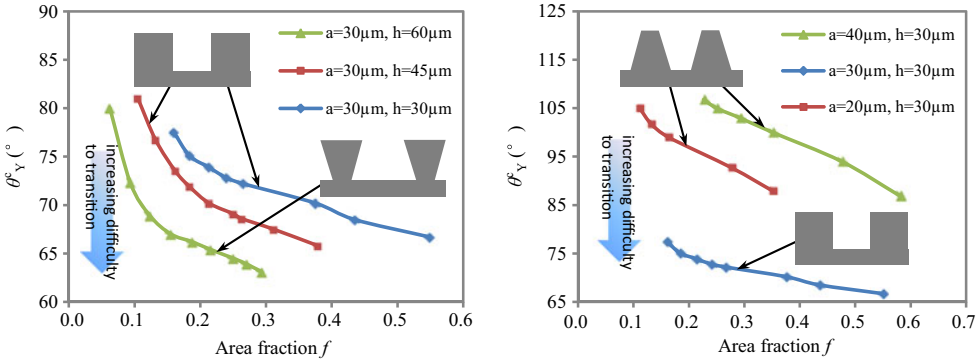

Fig. 5 Critical smooth-surface contact angle θ^c_Y vs area fraction f

transition occurred. Therefore, the above analysis and experimental results were in good agreement with Eq. 5.

With the external force ignored, p_c could be expressed as $p_c = p_L + p_G$, where p_G is the pressure generated by gravity of a droplet. Providing its impact on the apparent wetted area is homogenous, the gravity-generated pressure $p_G = \rho g V/\pi r^2_{wet}$ can be obtained. Regarding the droplet as a standard spherical cap, we can further express the radius r_{wet} of the apparent wetted area in terms of the droplet volume V and the contact angle θ in the following form:

$$r_{wet} = \left[\frac{3V}{\pi(1-\cos\theta)^2(2+\cos\theta)}\right]^{1/3}\sin\theta \tag{6}$$

In order to determine the dominant driving force for Cassie-Wenzel wetting transition between the Laplace's pressure p_L and the gravity-generated pressure p_G, a comparison between them using the same size of water droplets $V = 4$ μL was shown in Fig. 6. With the increasing of the contact angle θ, the Laplace's pressure p_L has an approximately linear enhancement within the scope of $0° < \theta < 120°$ and was almost constant at 145.7 ± 2.1 Pa within the scope of $120° \le \theta < 180°$, while the gravity-generated pressure p_G was much gently rising from 0 to 15.3 Pa within the scope of $0° < \theta < 120°$, increasing substantially from 15.3 to 192.0 Pa within the scope of $120° \le \theta < 165°$ and drastically growing from 192.0 Pa to infinity within the scope of $165° \le \theta < 180°$. It was found that

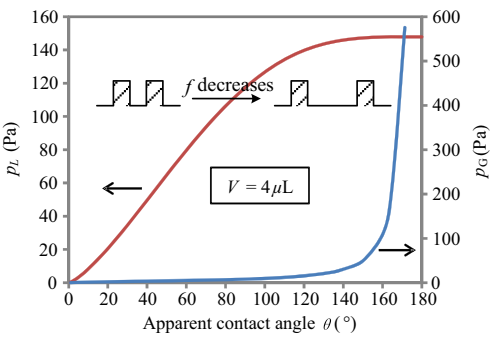

Fig 6 Apparent contact angle θ of a 4-μL water droplet on microstructured PDMS surfaces vs the Laplace' pressure p_L and the gravity-generated pressure p_G

p_L was dominant to p_G within the scope of $0° < \theta < 120°$, p_G was nonnegligible like p_L within the scope of $120° \le \theta < 165°$, and p_G was dominant to p_L within the scope of $165° < \theta < 180°$. According to the Cassie's equation, for water droplets on the microstructured PDMS surfaces ($\theta_Y = 109.6°$), the area fraction f will consequently diminish with the contact angle θ increasing, implying that the gravity-generated pressure p_G was, in the case of the area fraction $f < 0.176$ (calculated by $f = (1 + \cos\theta)/(1 + \cos\theta_Y)$ with $\theta = 152°$, obtaining $p_G = 58.0$ Pa, $p_L = 147.4$ Pa), a nonnegligible, even predominant, term for critical pressure p_c of Cassie-Wenzel transition.

Therefore, the gravity-generated pressure p_G should not be ignored under any circumstances. In this work, the gravity-generated pressure p_G would be taken into account for calculating pinning force. Then, according to Eq. 5, the following equation can be obtained:

$$\tau = \frac{1-f}{f}a^2(p_L + p_G) + 4a\gamma^c_{LV}\cos\theta^c_Y \tag{7}$$

Here, the parameter ψ is defined as the following form:

$$\psi = \left[2-\left(1+\cos\theta^c_Y\right)f\right]^{\frac{2}{3}}\left[1+\left(1+\cos\theta^c_Y\right)f\right]^{\frac{1}{3}} \tag{8}$$

Combining Eqs. 3, 6, 7, and 8 and the Cassie-Baxter equation, $\cos\theta = -1 + (1 + \cos\theta_Y)f$, yields the following equation:

$$\tau = \frac{1-f}{f}a^2\left(\gamma^c_{LV}\sqrt[3]{\frac{8\pi}{3V}}\psi + \rho^c g\sqrt[3]{\frac{V}{9\pi}}\psi^2\right) + 4a\gamma^c_{LV}\cos\theta^c_Y \tag{9}$$

This model determines pinning force τ in terms of such knowable parameters as area fraction f, side length a, droplet volume V, interfacial tension γ^c_{LV}, Young's contact angle θ^c_Y, and density ρ^c, which all could be directly measured by experimental apparatus.

According to Eq. 9, pinning force τ on different microstructured surfaces was obtained, as shown in Fig. 7. For the samples with square pillar-like microstructures, the pinning force τ was almost constant but has a slight increment with the increase of the area fraction f, owning averages of 1.66 μN for $a = 30$ μm, $h = 30$ μm, and 1.85 μN for $a = 30$ μm and $h = 45$ μm, which implies that larger height of

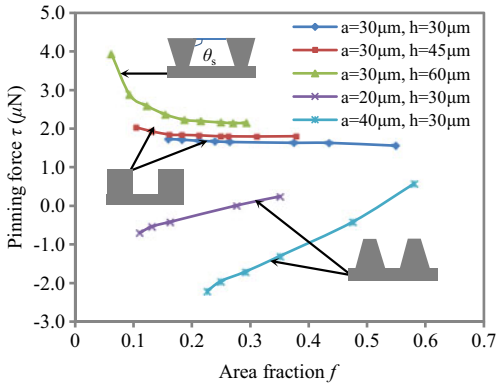

Fig. 7 Pinning force τ vs area fraction f

microstructure owns larger pinning force under the same f and a. However, for the samples decorated with similar inverted-trapezoid microstructures, the pinning force τ was almost constant with the scope of $0.188 < f < 0.293$, gradually increased with the scope of $0.094 < f < 0.188$, and significantly increased with the scope of $0.063 < f < 0.094$. Surprisingly, there were negative values of the pinning force of the samples with similar trapezoid microstructures, which may be caused by the shape of the microstructure, i.e., $\theta_s < 90°$. The pinning force of $a = 20$ μm and $h = 30$ μm was distinctly greater than the one of $a = 40$ μm and $h = 30$ μm, which means that a smaller scale of microstructure possesses greater pinning force under the same f and h. Moreover, there was no constant section but only approximately linear relationship. Nevertheless, it revealed that the pinning force of the samples can be intensely changed by the shape of the microstructure, i.e., the larger the shape angle θ_s was, the greater the pinning force τ was, under the same f and h. Ultimately, quantitative analysis was successfully applied to the pinning force, confirming the viewpoints and the rationality of the theoretical analysis in the section of pinning force.

To investigate the effect of the side length a and pinning force τ on the critical pressure p_c of different droplets for Cassie-Wenzel transition, we plot the theoretical values in Fig. 8 according to Eq. 5. It is easy to find from Fig. 8a that with the pinning force τ ignored, the droplets with Young's contact angle $\theta_Y < 90°$, such as pure ethanol and water-ethanol mixture droplets, are not able to maintain the Cassie state no matter how much the side length a, even their critical pressures p_c monotonously decrease with the decrease of the side length a, while the pure water droplet's behavior is on the contrary. When the pinning force τ is taken into account, under an arbitrarily fixed side length a, the critical pressures p_c of all droplets will increase with the increase of the pinning force τ, as shown in Fig. 8b–d. In addition, with the decrease of the side length a, the critical pressures p_c of the pure ethanol and water-ethanol mixture droplets first gently decrease and then sharply increase, resulting for each droplet a minimum value $p_{c,min}$, which corresponds to the critical side length a_{cr}. With the increase of the pinning force τ, the critical side length a_{cr} increases consequently, which implies that to gain the identical greater critical pressures p_c, we can properly increase the designed side length a to avoid the Euler instability [23] through enhancing the pinning force τ, such as optimizing the geometric shape of microstructures.

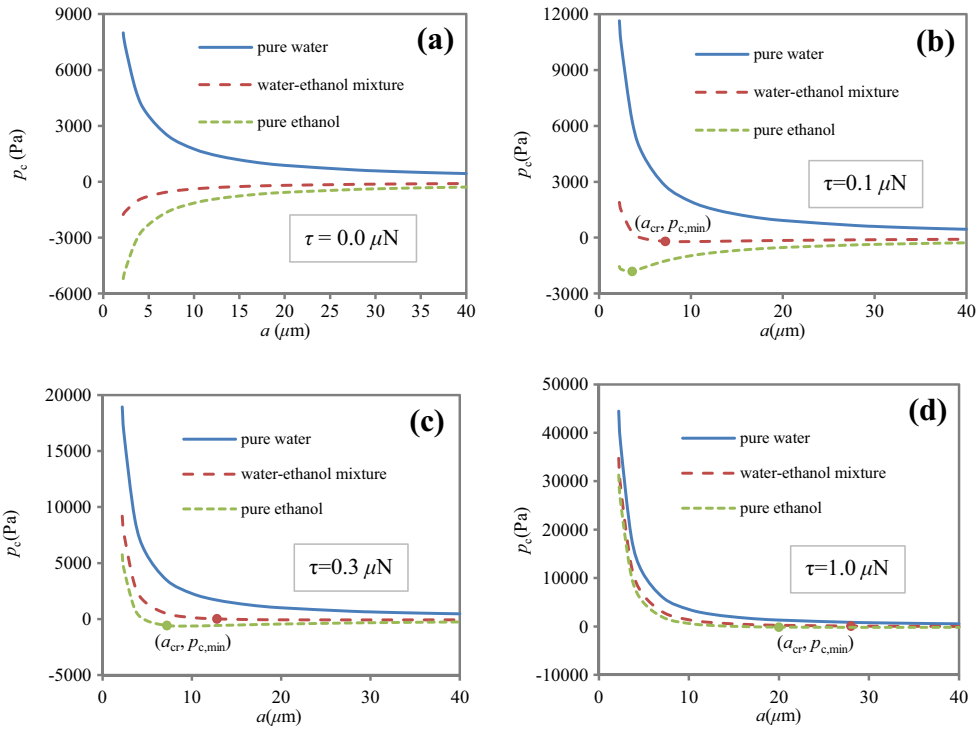

Fig. 8 Critical transition pressure p_c vs microstructure's side length a, under the condition of **a** $\tau = 0.0$ μN, **b** $\tau = 0.1$ μN, **c** $\tau = 0.3$ μN, and **d** $\tau = 1.0$ μN

Conclusions

The Cassie-Wenzel wetting transition on microstructured surfaces was investigated based on theoretical analysis and experimental observation. Using the pinning force τ, the model of critical pressure p_c of the Cassie-Wenzel wetting transition was obtained and the model was qualitatively verified by the experimental data. Moreover, the gravity-generated pressure p_G was, in the case of the area fraction $f < 0.176$, a nonnegligible even predominant term relative to the Laplace's pressure p_L for Cassie-Wenzel wetting transition. In consideration of both p_G and p_L, pinning force τ on the different microstructured surfaces was determined. It was found that the geometric size and shape could substantially enhance the magnitude of pinning force, such as scale-down of pillar's size and employment of a T-shape microstructure. Needs to be pointed out is that the droplet size here was in millimeter scale, its characteristic size was close to or greater than the capillary length, so the pressure p_G caused by the gravity of droplets was considered; otherwise, p_G was negligible.

Acknowledgments This study was funded by the National Natural Science Foundation of China (Grant No. 51176123), Specialized Research Fund for the Doctoral Program of Higher Education (Grant No. 20103120120006) and Shanghai Natural Science (Grant No. 11ZR1424800).

Compliance with ethical standards

Conflict of interest The authors declare that they have no conflict of interest.

References

1. Ren LQ, Wang SJ, Tian XM, Han ZW, Yan LN, Qiu ZM (2007) Non-smooth morphologies of typical plant leaf surfaces and their anti-adhesion effects. J Bionic Eng 4:33–40. doi:10.1016/S1672-6529(07)60010-9
2. Feng L, Li S, Li Y, Li H, Zhang L, Zhai J, Zhu D (2002) Superhydrophobic surfaces: from natural to artificial. Adv Mater 14:1857–1860. doi:10.1002/adma.200290020
3. Fürstner R, Barthlott W, Neinhuis C, Walzel P (2005) Wetting and self-cleaning properties of artificial superhydrophobic surfaces. Langmuir 21:956–961. doi:10.1021/la0401011
4. Bhushan B, Jung YC (2011) Natural and biomimetic artificial surfaces for superhydrophobicity, self-cleaning, low adhesion, and drag reduction. Prog Mater Sci 56:1–108. doi:10.1016/j.pmatsci.2010.04.003
5. Kim P, Wong TS, Alvarenga J, Kreder MJ, Adorno-Martinez WE, Aizenberg J (2012) Liquid-infused nanostructured surfaces with extreme anti-ice and anti-frost performance. ACS Nano 6:6569–6577. doi:10.1021/nn302310q
6. Tsukamoto K, Uchikoshi J, Goto S, Kawase T, Ajari N, Nagai T, Morita M (2010) Photoetching of silicon by N-fluoropyridinium Salt. Electrochem Solid-State Lett 13:D80–D82. doi:10.1149/1.3481770
7. Zhao H, Park KC, Law KY (2012) Effect of surface texturing on superoleophobicity, contact angle hysteresis, and "robustness". Langmuir 28:14925–14934. doi:10.1021/la302765t
8. Teshima K, Sugimura H, Inoue Y, Takai O, Takano A (2005) Transparent ultra water-repellent poly (ethylene terephthalate) substrates fabricated by oxygen plasma treatment and subsequent hydrophobic coating. Appl Surf Sci 244:619–622. doi:10.1016/j.apsusc.2004.10.143
9. Wang Y, Wang W, Zhong L, Wang J, Jiang Q, Guo X (2010) Superhydrophobic surface on pure magnesium substrate by wet chemical method. Appl Surf Sci 256:3837–3840. doi:10.1016/j.apsusc.2010.01.037
10. Bellanger H, Darmanin T, Taffin de Givenchy E, Guittard F (2014) Chemical and physical pathways for the preparation of superoleophobic surfaces and related wetting theories. Chem Rev 114:2694–2716. doi:10.1021/cr400169m
11. Zhang X, Shi F, Niu J, Jiang Y, Wang Z (2008) Superhydrophobic surfaces: from structural control to functional application. J Mater Chem 18:621–633. doi:10.1039/B711226B
12. Whyman G, Bormashenko E (2011) How to make the Cassie wetting state stable? Langmuir 27:8171–8176. doi:10.1021/la2011869
13. Groten J, Rühe J (2013) Surfaces with combined microscale and nanoscale structures: a route to mechanically stable superhydrophobic surfaces? Langmuir 29:3765–3772. doi:10.1021/la304641q
14. San-Miguel A, Behrens SH (2012) Influence of nanoscale particle roughness on the stability of Pickering emulsions. Langmuir 28:12038–12043. doi:10.1021/la302224v
15. Varnik F, Gross M, Moradi N, Zikos G, Uhlmann P, Müller-Buschbaum P, Stamm M (2011) Stability and dynamics of droplets on patterned substrates: insights from experiments and lattice Boltzmann simulations. J Phys Condens Matter 23:184112. doi:10.1088/0953-8984/23/18/184112
16. Lei W, Jia ZH, He JC, Cai TM, Wang G (2014) Vibration-induced Wenzel-Cassie wetting transition on microstructured hydrophobic surfaces. Appl Phys Lett 104:181601. doi:10.1063/1.4875586
17. Lei W, Jia ZH, He JC, Cai TM (2014) Dynamic properties of vibrated drops on a superhydrophobic patterned surface. Appl Therm Eng 62:507–512. doi:10.1016/j.applthermaleng.2013.10.019
18. Liu G, Craig VS (2010) Macroscopically flat and smooth superhydrophobic surfaces: heating induced wetting transitions up to the Leidenfrost temperature. Faraday Discuss 146:141–151. doi:10.1039/B924965F
19. Liu G, Fu L, Rode AV, Craig VS (2011) Water droplet motion control on superhydrophobic surfaces: exploiting the Wenzel-to-Cassie transition. Langmuir 27:2595–2600. doi:10.1021/la104669k
20. Krupenkin TN, Taylor JA, Wang EN, Kolodner P, Hodes M, Salamon TR (2007) Reversible wetting-dewetting transitions on electrically tunable superhydrophobic nanostructured surfaces. Langmuir 23:9128–9133. doi:10.1021/la7008557
21. Kumari N, Garimella SV (2011) Electrowetting-induced dewetting transitions on superhydrophobic surfaces. Langmuir 27:10342–10346. doi:10.1021/la2027412
22. Cheng Z, Lai H, Zhang N, Sun K, Jiang L (2012) Magnetically induced reversible transition between Cassie and Wenzel states of superparamagnetic microdroplets on highly hydrophobic silicon surface. J Phys Chem C 116:18796–18802. doi:10.1021/jp304965j
23. Zheng QS, Yu Y, Zhao ZH (2005) Effects of hydraulic pressure on the stability and transition of wetting modes of superhydrophobic surfaces. Langmuir 21:12207–12212. doi:10.1021/la052054y
24. Patankar NA (2004) Transition between superhydrophobic states on rough surfaces. Langmuir 20:7097–7102. doi:10.1021/la049329e

25. Ishino C, Okumura K, Quéré D (2004) Wetting transitions on rough surfaces. EPL (Europhysics Letters) 68:419. doi:10.1209/epl/i2004-10206-6
26. Murakami D, Jinnai H, Takahara A (2014) Wetting transition from the Cassie–Baxter state to the Wenzel state on textured polymer surfaces. Langmuir 30:2061–2067. doi:10.1021/la4049067
27. Ren W (2014) Wetting transition on patterned surfaces: transition states and energy barriers. Langmuir 30:2879–2885. doi:10.1021/la404518q
28. Jung YC, Bhushan B (2007) Wetting transition of water droplets on superhydrophobic patterned surfaces. Scr Mater 57:1057–1060. doi:10.1016/j.scriptamat.2007.09.004
29. Giacomello A, Meloni S, Chinappi M, Casciola CM (2012) Cassie–Baxter and Wenzel states on a nanostructured surface: phase diagram, metastabilities, and transition mechanism by atomistic free energy calculations. Langmuir 28:10764–10772. doi:10.1021/la3018453
30. Bormashenko E, Musin A, Whyman G, Zinigrad M (2012) Wetting transitions and depinning of the triple line. Langmuir 28:3460–3464. doi:10.1021/la204424n
31. Gao N, Yan Y (2009) Modeling superhydrophobic contact angles and wetting transition. J Bionic Eng 6:335–340. doi:10.1016/S1672-6529(08)60135-3
32. Xu X, Vereecke G, Chen C, Pourtois G, Armini S, Verellen N, De Gendt S (2014) Capturing wetting states in nanopatterned silicon. ACS Nano 8:885–893. doi:10.1021/nn405621w
33. Vogler EA (1998) Structure and reactivity of water at biomaterial surfaces. Adv Colloid Interf Sci 74:69–117. doi:10.1016/S0001-8686(97)00040-7
34. Berg JM, Eriksson LT, Claesson PM, Borve KGN (1994) Three-component Langmuir-Blodgett films with a controllable degree of polarity. Langmuir 10:1225–1234. doi:10.1021/la00016a041
35. Forsberg PS, Priest C, Brinkmann M, Sedev R, Ralston J (2009) Contact line pinning on microstructured surfaces for liquids in the Wenzel state. Langmuir 26:860–865. doi:10.1021/la902296d
36. Fetzer R, Ralston J (2011) Exploring defect height and angle on asymmetric contact line pinning. J Phys Chem C 115:14907–14913. doi:10.1021/jp203581j
37. Pilat DW, Papadopoulos P, Schaffel D, Vollmer D, Berger R, Butt HJ (2012) Dynamic measurement of the force required to move a liquid drop on a solid surface. Langmuir 28:16812–16820. doi:10.1021/la3041067
38. Hong SJ, Chang FM, Chou TH, Chan SH, Sheng YJ, Tsao HK (2011) Anomalous contact angle hysteresis of a captive bubble: advancing contact line pinning. Langmuir 27:6890–6896. doi:10.1021/la2009418
39. Wang FC, Wu HA (2013) Pinning and depinning mechanism of the contact line during evaporation of nano-droplets sessile on textured surfaces. Soft Matter 9:5703–5709. doi:10.1039/C3SM50530H
40. Ahuja A, Taylor JA, Lifton V, Sidorenko AA, Salamon TR, Lobaton EJ, Krupenkin TN (2008) Nanonails: a simple geometrical approach to electrically tunable superlyophobic surfaces. Langmuir 24:9–14. doi:10.1021/la702327z